



Article

Research on Insurance Method for Energetic Materials on Information Self-Destruction Chips

Hengzhen Feng , Wenzhong Lou , Bo He, Sining Lv and Wenting Su

School of Mechatronical Engineering, Beijing Institute of Technology, Beijing 100811, China; cqrrhb0928@126.com (B.H.); lvsining@bit.edu.cn (S.L.); 3120210187@bit.edu.cn (W.S.)

* Correspondence: fenghengzhen@gmail.com (H.F.); louwz@bit.edu.cn (W.L.); Tel.: +86-010-18813173812 (H.F.)

Abstract: Detonation waves released by energetic materials provide an important means of physical self-destruction (Psd) for information storage chips (ISCs) in the information insurance field and offer advantages that include a rapid response and low driving energy. The high electrical sensitivity of energetic materials means that they are easily triggered by leakage currents and electrostatic forces. Therefore, a Psd module based on a graphene-based insurance actuator heterogeneously integrated with energetic materials is proposed. First, the force–balance relation between the electrostatic van der Waals force and the elastic recovery force of the insurance actuator’s graphene electrode is established to realize physical isolation and an electrical interconnection between the energetic materials and the peripheral electrical systems. Second, a numerical analysis of the detonation wave stress of the energetic materials in the air domain is performed, and the copper azide dosage required to achieve reliable ISC Psd is obtained. Third, the insurance actuator is prepared via graphene thin film processing and copper azide is prepared via an in situ reaction. The experimental results show that the energetic materials proposed can release physical isolation within 14 μ s and can achieve ISC Psd under the application of a voltage signal (4.4–4.65 V). Copper azide (0.45–0.52 mg) can achieve physical damage over an ISC area (23.37–35.84 mm²) within an assembly gap (0.05–0.25 mm) between copper azide and ISC. The proposed method has high applicability for information insurance.

Keywords: energetic materials; information insurance; physical self-destruction; insurance actuator; physical isolation



Citation: Feng, H.; Lou, W.; He, B.; Lv, S.; Su, W. Research on Insurance Method for Energetic Materials on Information Self-Destruction Chips. *Micromachines* **2022**, *13*, 875. <https://doi.org/10.3390/mi13060875>

Academic Editors: Ha Duong Ngo and Aiqun Liu

Received: 14 April 2022

Accepted: 30 May 2022

Published: 31 May 2022

Publisher’s Note: MDPI stays neutral with regard to jurisdictional claims in published maps and institutional affiliations.



Copyright: © 2022 by the authors. Licensee MDPI, Basel, Switzerland. This article is an open access article distributed under the terms and conditions of the Creative Commons Attribution (CC BY) license (<https://creativecommons.org/licenses/by/4.0/>).

1. Introduction

Physical self-destruction (Psd) represents an important method to improve the information insurance performance of information storage chips (ISCs) [1,2]. The German Federal Ministry of Education and Research invested more than €25 million in the ZEUS Trusted Electronics Program in 2020, which is dedicated to developing the information insurance for information storage chips [3]. Under the support of this project, the Psd module with a multi-sensor stack was developed by Fraunhofer Institute. To date, numerous research institutions have announced a variety of schemes (e.g., using high-voltage excitation, electrochemical degradation, detonation stress waves, and other methods) to achieve the Psd of ISCs. For example, the US Defense Advanced Research Projects Agency (DARPA) launched the Vanishing Programmable Resources (VAPR) project in 2013 [4]. According to the self-destruction requirements for military-grade electronic equipment that were developed by the US military, the VAPR project [5] was based on a “pressure release trigger decomposition” approach, which was intended to verify that military electronic systems had the ability to be destroyed in a physical manner; this would prevent the leakage of secret information and manufacturing processes after reverse engineering of the core electronic devices. In 2015, the Xerox Palo Alto Research Center released a self-destructing chip [6]. The mechanism was triggered by a laser or wireless signal, causing the chip to heat up and crack the electronic device by heat accumulation. After the thermal

shock occurred, the substrate broke within a few seconds, and the device could then not be restored. However, these methods relied on the application of external high-power energy, e.g., laser signals, and thus, apply to a limited number of scenarios. Therefore, energetic materials [7,8] have been used to generate detonation waves (GPa level) in microseconds via voltage excitation (below 5 V) to achieve Psd. However, because of the low driving thresholds of these energetic materials, the improvement of the anti-interference capabilities of these materials has become another core issue in this field. Many anti-interference ability protection measures use a transient voltage suppression (TVS) diode [9–12] to absorb transient energy. The voltage clamp was applied between two poles and was set at a predetermined value that could not be adjusted for use under different environments [13–16], but its energy absorption performance was limited [17,18]. In 2020, the Beijing Institute of Technology announced OFF-ON-OFF microelectromechanical systems based on a modified Paschen's law [19]; in this system, a comb-shaped actuator (electrode gap: 1–10 μm) was able to reduce the threshold voltage to 130 V for air breakdown [19], and the electrical state was switched in an OFF-ON-OFF sequence to complete energy grooming for abnormal interference signals. In addition, a metal-based "OFF-ON" actuator was designed based on corona discharge theory to achieve air breakdown at a threshold voltage [20–23]. These schemes can be used to provide an energy grooming function to achieve insurance control of the energetic materials. However, the threshold voltage generally still exceeds 45 V [24,25], which represents a comparatively high energy burden for Psd modules. In contrast, only the "ON-OFF" actuator offers the advantage of low voltage operation. In 2010, Rossi from LAAS in France developed three actuators: an electrothermal evaporation-breaking solid actuator, an electro-explosion-breaking solid actuator, and an electrothermal welding-conducting solid actuator. These three actuator types mainly rely on the thermal accumulation of their metal electrodes. This thermal energy acts on the sensitive mechanism of the actuator [26,27], causing electrode melting/vaporization and other phenomena. The voltage pulses for these actuators are distributed over a range from 3.3 V to 8 V, and the response times of the actuator states (i.e., ON-OFF) are on the microsecond scale. In 2014, Beijing Institute of Technology presented a solid-state actuator based on a multilayer metal stack. This type of actuator can melt out completely under a threshold voltage of 1.5 V. The response time distribution for the actuator ranges from 10 ms to 150 ms [28,29]. These actuators can only isolate the energetic materials from the peripheral electrical system by parallel connections, but the isolation method is only intended to provide electrical isolation, and thus, cannot shield the materials from the effects of the leakage currents. Therefore, based on the insurance requirements for energetic materials discussed above, this paper presents an insurance actuator that provides physical isolation from peripheral electrical systems through functional integration with the energetic materials, which also reduces triggering of the materials by leakage currents. The proposed technique has a strong practical application value.

2. Theory

2.1. Design of Insurance Actuator Model for Energetic Materials

In this paper, ISC Psd is achieved using a detonation wave that is generated by energetic materials in a micro-region and propagates in the air domain. The scheme offers advantages that include small device size, low driving energy requirements, and fast response times. The energetic materials are mainly composed of a semiconductor bridge (SCB) and copper azide. The detonation wave for copper azide requires high-temperature plasma that is released by the SCB. When the external electrical signal acts on the SCB, the bridge region goes through a solid heating–liquid heating–silicon gasification–silicon vapor ionization sequence to form a high-temperature plasma. This high-temperature plasma is diffused into the copper azide by micro-convection and thus realizes the detonation energy output. However, because of the limitations of the high electrostatic sensitivity of copper azide, it can also be easily driven by external leakage currents or electrostatic, thus resulting in false triggering. Therefore, this paper presents the design of a Psd module based on

matching the design of the insurance actuator and the energetic materials. If the physical isolation and connection between energetic materials and the peripheral electrical systems can be achieved, the insurance of energetic materials can be improved.

The insurance actuator consists of a three-layer graphene electrode that is stacked together with a dielectric layer and is connected in series with the SCB, as illustrated in Figure 1. The insurance actuator has “absorption” and “isolation” states. In these two states, the “absorption” state represents the interconnection of the energetic materials with the peripheral electrical systems, and the “isolation” state represents the physical isolation of the energetic materials from the peripheral electrical systems. The ISC self-destruction mechanism based on the energetic materials and the insurance actuator is described as follows and is shown in Figure 2.

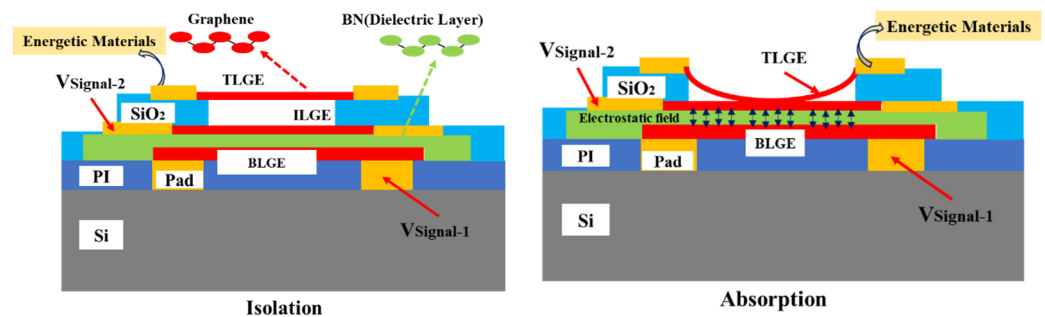


Figure 1. Functional matching model of insurance actuator and energetic materials.

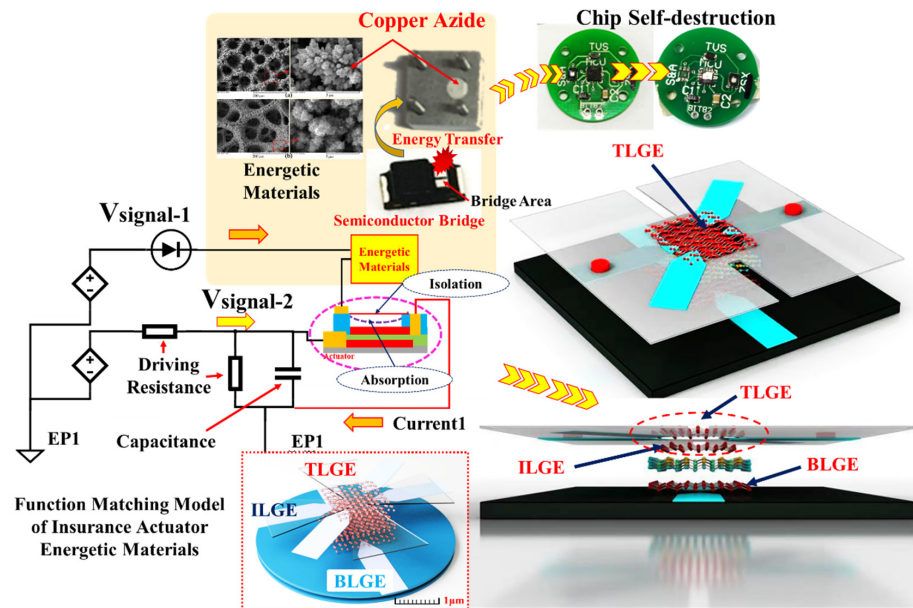


Figure 2. ISC self-destruction mechanism based on energetic materials and insurance actuator.

The bottom graphene electrode induces $V_{\text{signal-1}}$, an electric field that can be generated between the bottom layer graphene electrode (BLGE) and the boron nitride dielectric layer. The top layer graphene electrode (TLGE) induces an electrostatic van der Waals force to overcome the elastic recovery force and makes contact with the intermediate layer graphene electrode (ILGE). At this time, the energetic materials are connected in series with the peripheral electrical system. When the ILGE induces $V_{\text{signal-2}}$, the SCB then produces a high-temperature plasma that is used to drive the copper azide. Finally, the copper azide releases the detonation wave, which is then transferred to the ISCs, allowing for the Psd to be achieved. In addition, when $V_{\text{signal-1}}$ is reset, the electric field in the dielectric layer then vanishes. The TLGE resets under the action of the elastic recovery force alone, thus causing

the energetic materials to be isolated physically from the peripheral electrical system. Due to the appropriate functional matching design between the actuator and the energetic materials, the energetic materials are suitable for use within the information insurance field.

To achieve TLGE absorption, it is important to build a balance relation between the electrostatic van der Waals force and the elastic recovery force. A force-balance equation is constructed as shown in Equation (1), and the elastic recovery force is described using Equation (2):

$$F_{re} = kd = n \frac{8Ewt^3}{L^3}(l - z) \tag{1}$$

$$F_{Con} = F_{van} - F_{re} = \frac{A_H A}{12\pi z^2} - kd = \frac{A_H A}{12\pi z^2} - n \frac{8Ewt^3}{L^3}(l - z) \tag{2}$$

In these equations, E is Young’s modulus for graphene, w , t , and L are the width, thickness, and length of the TLGE, respectively, and z is the gap between the TLGE and the ILGE. Additionally, A_H is the Hamaker constant of graphene, which is taken to be 4.7×10^{-19} J, A is the contact area, and K is the spring constant of the graphene beam.

To increase the TLGE motion displacement, this paper proposes four electrode models in combination with the mechanical relation given in Equation (1). The relationship between the electrode length and the motion displacement was obtained as shown in Figure 3, and a mechanical simulation analysis of the TLGE was performed as shown in Figure 4.

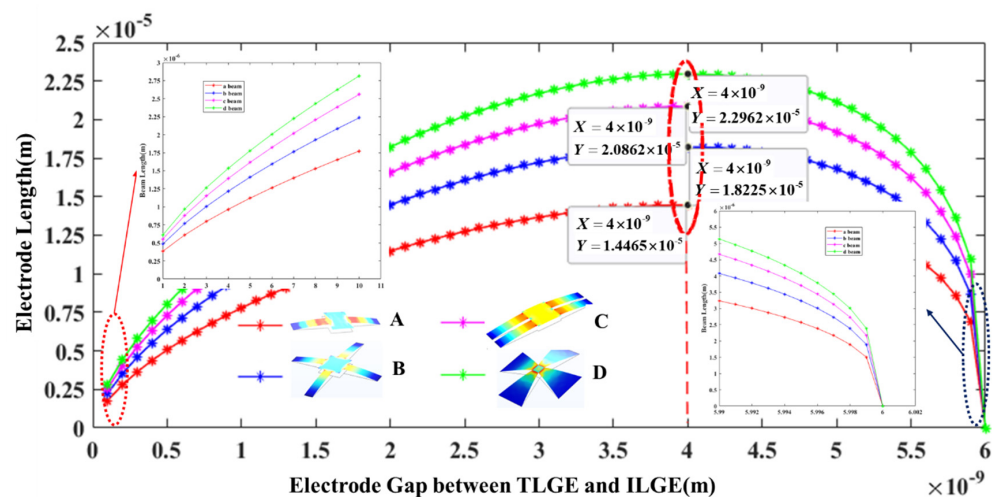


Figure 3. Relationship between the electrode length and the motion displacement.

According to Figure 3, the four models show a trend that when the gap between the TLGE and the ILGE increases, the length of the TLGE initially increases and then decreases. When this gap is 4 nm, the length of the D model is the longest at 22.96 μm , which is longer than all the other models.

In this paper, the von mises and displacement numerical analyses of four models are carried out under the gap (4 nm) between the TLGE and the ILGE in Figure 4.

When the TLGE induced the electrostatic Van der Waals force for 1 μs , the A model produces the maximum von mises and motion displacement (10.4 MPa, 0.14 μm), the C model produces the minimum von mises and motion displacement (1.44 MPa, 0.08 μm), in which the maximum von mises is less than the graphene fracture strength, and the minimum displacement is greater than 4 nm. It can be seen that the four TLGE models of the insurance actuator can satisfy the transformation from the “absorption” to “isolation” states under steady-state conditions. The relationships among the “absorption” time, the electrode model, and the displacement are analyzed, with the results illustrated in Figure 5.

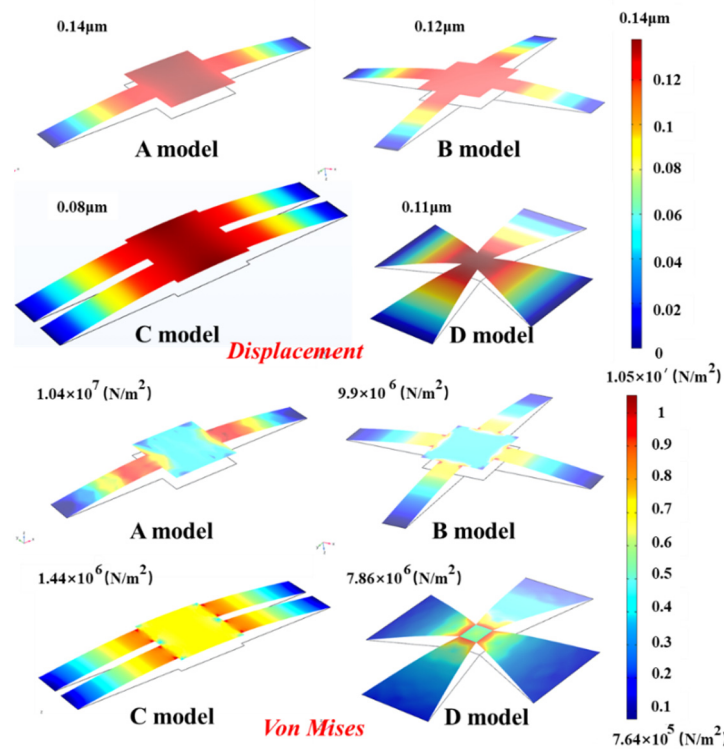


Figure 4. Mechanical simulation analysis of the TLGE.

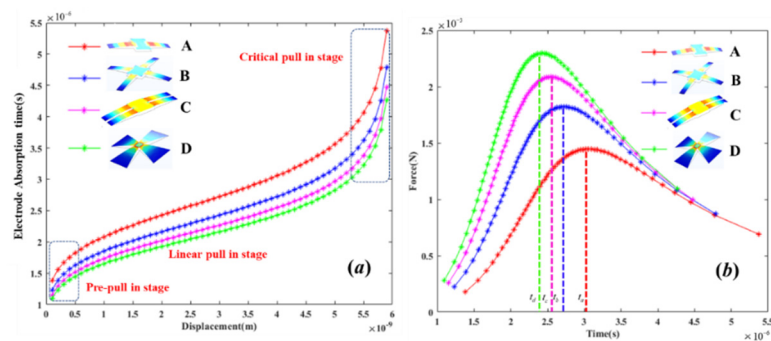


Figure 5. Relationships among absorption time, electrode model, and displacement. (a) Relationship between absorption time and displacement for four models. (b) Relationship between Force and absorption time for four models.

According to Figure 5, under the same displacement conditions, the graphene electrode (D model) shows the shortest motion response time of 4.47 μs . The absorption time with the A model is 5.5 μs . In addition, when using the D model as an example, the absorption time of the TLGE consists of three stages: the pre-suction stage, the liner suction stage, and the critical suction stage.

When the electrode induces an electrostatic van der Waals force and the displacement is within the 0–0.5 nm range, the absorption time is close to 1.5 μs , and the velocity of the movement is 0.25×10^{-3} m/s. When the displacement is in the range from 0.5 nm to 5.3 nm, the absorption time shows a linear trend, and the maximum velocity reaches 3.2×10^{-3} m/s. Subsequently, when the TLGE moves toward the ILGE, the TLGE velocity falls to 0.47×10^{-3} m/s. In other words, the TLGE’s motion is constrained strongly by the electrostatic field and the restoring force during the initial and final stages, respectively.

According to Figure 5b, the resultant force acting on the TLGE increases before weakening during the absorption state, and the complete movement process can be divided into two distinct sections. Using the D model as an example, during the period from 0 to

2.5 μs , the resultant force increases, thus causing the displacement gradient to increase. Then, during the period from 2.5 to 4.5 μs , the displacement gradient decreases, with the resultant force also decreasing. The resultant force in the D model is greater than that in the other electrode models, where the maximum absorption time follows the relation $t_A > t_B > t_C > t_D$. In summary, the D model is used for the TLGE. The electrode thickness was calculated to be 0.68 nm, and the contact area for the top electrode layer is $1.69 \mu\text{m}^2$.

2.2. Design of Energy Transfer Model for Energetic Materials

The Psd module proposed in this paper mainly includes the charge mechanism, the SCB, copper azide, and the ISCs. Copper azide represents the core self-destruction element and relies on an in situ reaction. The transmission of the detonation stress wave is performed based on a high-speed combustion material model. The dimensions of the copper azide element are $\text{Ø}1 \times 0.5 \text{ mm}^2$, and the charge dose is in the 0.45–0.52 mg range. The stress wave of the copper azide energy transfer process over time is shown in Figure 6. A simplified model of the assembly relationship between the copper azide and the ISC is shown in Figure 6a [30].

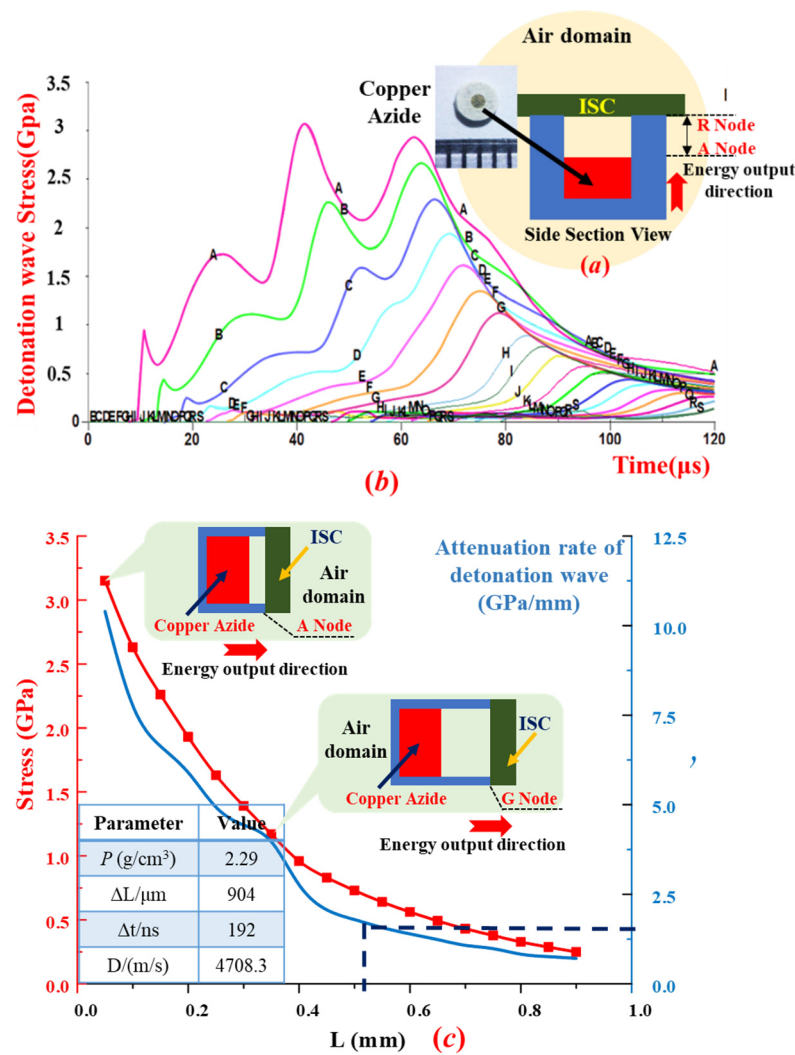


Figure 6. Stress wave of copper azide energy transfer over time. (a) The model of Psd module. (b)detonation wave stress variation curve by time in air domain. (c) The relationship between detonation wave stress, attenuation rate under different air gap.

The assembly gap between these two elements is used to enhance the growth of the detonation wave in the air domain such that it strikes the surface of the ISC with sufficiently

high intensity to achieve ISC Psd. In this paper, the transmission analysis of the detonation waves in the air domain is achieved with the aid of LS-DYNA software, with results as shown in Figure 6b.

According to the results in Figure 6b, the air gap between the copper azide in the energetic material and the ISC can be divided into 17 nodes (A–R nodes), where the gap between adjacent nodes is 0.05 mm. The stress versus time relationship can be obtained from the LS-DYNA analysis: the stress at each node in the air domain increases initially and then decreases, and the stress wave attenuates rapidly beyond the backward position of the node.

In combination with the structural critical strength (1 GPa) of the plastic chip, when the assembly gap is 0.05 mm (A node), the maximum stress in the air domain reaches 3.15 GPa, and its duration is 25 μ s; however, when the assembly gap is 0.35 mm (G node), the maximum stress in the air domain reaches 1.25 GPa, and the duration is 11 μ s. In this paper, the A–G node is selected as the upper limit of the air gap between the copper azide and the ISC assembly.

Figure 6c shows the stress attenuation relationship of the detonation wave at each node in the air domain. When the node is located within the A–G range, the attenuation rate of the detonation wave reaches 4.2–10.4 GPa/mm. When the node is located within the H–R range, the stress wave attenuation rate then reaches 0.7–2.6 GPa/m. In other words, because of the serious attenuation of the stress during the initial stage (from the A node), the stress value at the H–R node is not sufficient to achieve ISC Psd. Therefore, the assembly gap between the copper azide and the ISC must be in the 0.05–0.25 mm range.

3. Experimental

As shown in Figure 7, the fabrication process flow includes two modules.

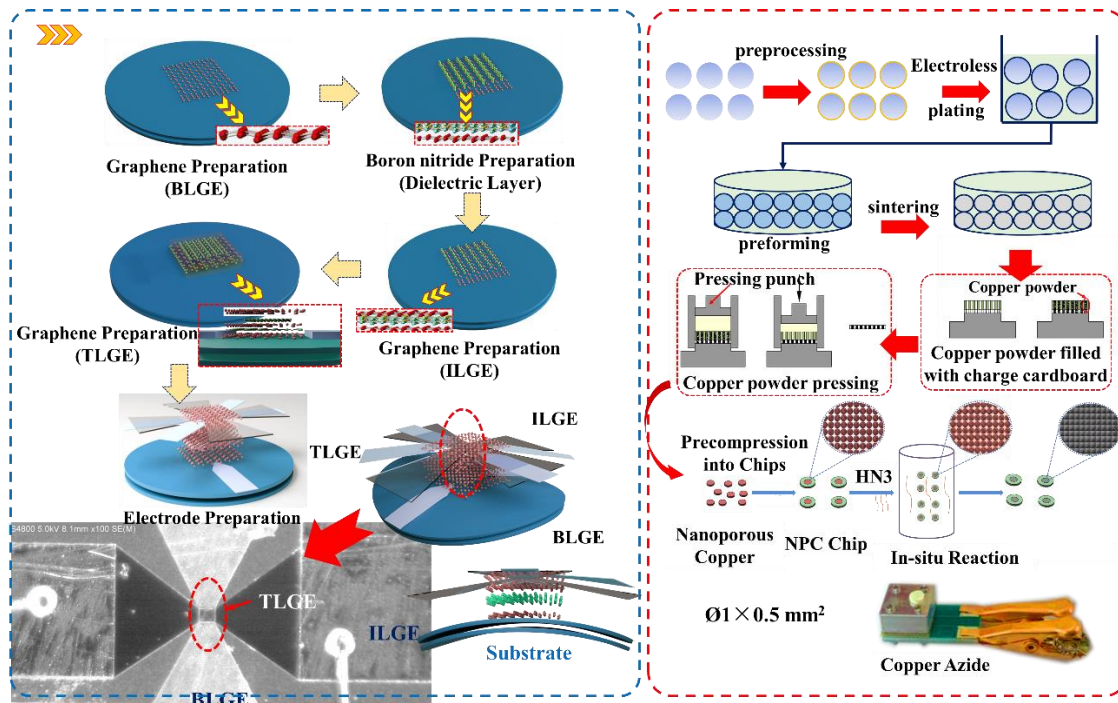


Figure 7. Fabrication processes of insurance actuator and copper azide.

MI. Preparation process for the insurance actuator.

Step I. Graphene (thickness: 0.46 nm) is mechanically exfoliated from highly-directional pyrolyzed graphite onto silicon wafers that have been thermally oxidized to have a SiO_2 film (40 nm) coating. The BLGE is then patterned via ion beam lithography to form the electrostatic induction unit of the insurance actuator.

Step II. A boron nitride layer (1.3 nm) is sputtered onto the BLGE, and the electrostatic field induction region is realized via lithographic processing.

Step III. A graphene (0.46 nm) electrode is prepared via a similar process (see Step I) on top of the boron nitride layer, forming the ILGE, which is then patterned by ion beam lithography.

Step IV. A SiO₂ mask is formed by plasma-enhanced chemical vapor deposition (CVD) on the ILGE; this layer then forms the gap between the TLGE and the ILGE.

Step V. The TLGE (0.46 nm) is mechanically striped on the top of the SiO₂ layer via ion beam lithography, and the SiO₂ mask is etched using a buffered HF solution to release the gap between the ILGE and the TLGE. Finally, the BLGE, the ILGE, and the TLGE pad, which connect in series with the peripheral electrical system, are formed by evaporation of Pt onto the actuator surface.

MII. Preparation process for the copper azide.

Step I. First, polystyrene (PS) microspheres are selected as templates; microspheres (PS/Cu) are prepared by electroless Cu plating on the PS microsphere surfaces. Second, these PS/Cu microspheres are preformed and sintered at 400 °C in N₂ and air, respectively. Finally, hollow Cu microspheres (thickness: 100 nm) and hollow CuO microspheres (thickness: 200 nm) are prepared.

Step II. The Cu and CuO microspheres are then pressed into a charging mechanism to form a nanoporous copper layer.

Step III. A nanoporous copper chip is then formed by pre-pressing of a cartridge ring.

Step IV. An in situ reaction with HN₃ is performed at 55 °C for 24 h to create the copper azide.

The process above thus verified that copper azide can be prepared successfully via the proposed in situ reaction.

The insensitive SCB, which has a strong overcurrent ability, was selected in this study. This SCB can improve the insurance of copper azide, and the resistance in the bridge area was between 1.1–1.2 Ω.

4. Test and Measurement

According to the mechanism illustrated in Figure 2, the absorption behavior in the insurance actuator test was measured under various driving voltages ($V_{\text{signal-1}} = 1.30\text{--}2.10\text{ V}$). In addition, multiple absorption fatigue test cycles were performed at the same driving voltage, and the relationship between the TLGE absorption time and the number of test cycles was obtained, as shown in Figure 8.

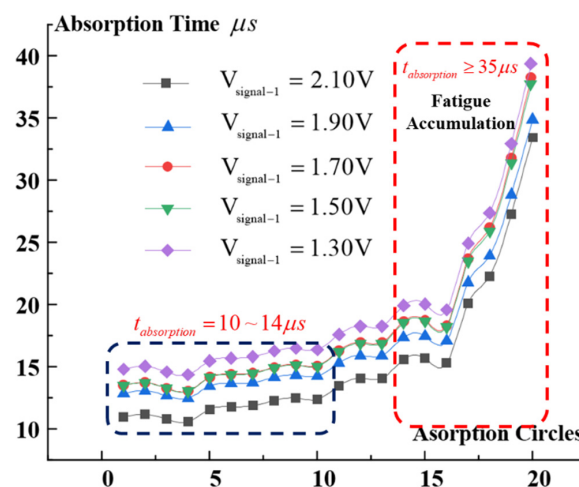


Figure 8. Absorption time changes with driving voltage and number of test cycles.

Over the same number of test cycles (cycles = 1–14), the driving voltage ($V_{\text{signal-1}}$) of the BLGE gradient ranges from 1.30 V to 2.10 V, and the absorption time of the TLGE decreases, with a distribution within the 10–14 μs range. Under the same driving voltage, the absorption time increases with increasing numbers of cycles. When the number of cycles reaches 20, the absorption time then exceeds 35 μs .

Based on the experimental conclusions drawn above, the dosage of copper azide is 0.52 mg; the Psd test results obtained for the ISCs are shown in Figure 9. When the number of cycles = 5, $V_{\text{signal-1}} = 1.728$ V, and $V_{\text{signal-2}} = 4.56$ V, the Psd time (from TLGE absorption to detonation wave generation) is 10 μs . When the number of cycles = 15, $V_{\text{signal-1}} = 2.1$ V, and $V_{\text{signal-2}} = 4.48$ V, the Psd time is 14 μs . In summary, when the number of cycles ranged from 1 to 14, the variation in the Psd response time was only 40%. When the number of cycles reached 20, the Psd time reached 32 μs , which is 2.2 times longer than the original Psd time, and the mechanical response of the TLGE showed fatigue accumulation behavior.

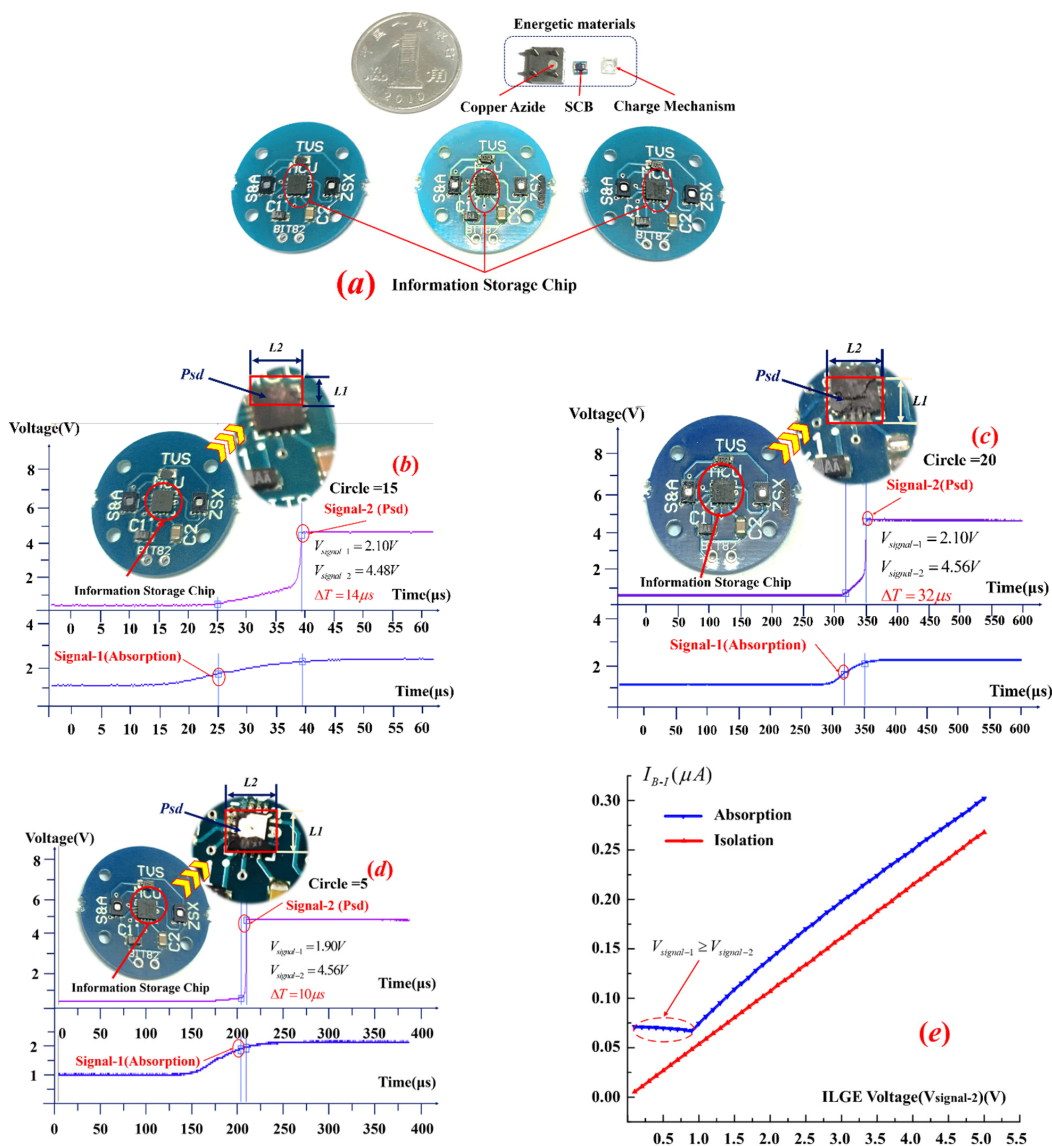


Figure 9. (a) ISC Psd module, (b–d) Psd times for different numbers of test cycles, and (e) leakage currents between the BLGE and the ILGE under the absorption/isolation states.

In addition, the leakage currents between the bottom and interlayer electrodes were measured in both the absorption and isolation states, and the experimental results are shown in Figure 9d.

As Figure 9e shows, when the actuator is in the absorption state, the leakage current (I_{B-I}), which is distributed from 0.068 to 0.073 μA within the $V_{\text{signal-2}}$ range from 0 to 0.9 V, decreases. The main reason for this behavior is that the driving voltage of the BLGE ($V_{\text{signal-1}}$) is higher than that of the ILGE ($V_{\text{signal-2}}$), and their currents are in opposite directions. The leakage current is offset with increasing $V_{\text{signal-2}}$, and when $V_{\text{signal-2}}$ exceeds 0.9 V, the leakage current increases linearly with increasing voltage, with the linear rate of increase reaching 0.062 $\mu\text{A}/\text{V}$. When the TLGE is in the isolation state, the leakage current increases linearly with increasing $V_{\text{signal-2}}$, and the linear rate of increase reaches 0.053 $\mu\text{A}/\text{V}$.

In addition, the Psd area of the ISC was calibrated for 10 groups, with results as shown in Table 1.

Table 1. The Psd area of the ISC.

	1	2	3	4	5	6	7	8	9	10
$L_1(\text{mm})$	6.3	5.8	4.7	6.4	6.9	4.8	5.6	6.7	4.5	5.7
$L_2(\text{mm})$	4.5	5.9	6.4	4.6	4.8	6.1	6.4	3.7	5.9	4.1

In summary, copper azide (0.52 mg) can achieve physical damage over an ISC area of 23.37–35.84 mm^2 and the Psd of the ISC within an assembly gap range of 0.05–0.25 mm. The proposed scheme has extensive application value in information insurance.

5. Conclusions

In this paper, energetic materials are used to achieve ISC Psd. To prevent the energetic materials from being influenced by leakage currents, a graphene-based insurance actuator is proposed. During matching testing between the actuator and the energetic materials, it was concluded that the minimum absorption time for the TLGE is 10 μs . When the number of absorption/isolation cycles ranged from 1 to 14, the variation in the Psd response time was only 40%. When the number of cycles reached 20, the Psd time reached 32 μs , which is 2.2 times longer than the original Psd time, and the mechanical response of the TLGE showed fatigue accumulation. In addition, when $V_{\text{signal-1}}$ was 2.10 V, $V_{\text{signal-2}}$ reached 4.56 V, the TLGE was in the absorption state, and ISC Psd could be achieved, with the maximum leakage current for the insurance actuator reaching 0.302 μA . Additionally, when the TLGE was isolated, the maximum leakage current was 0.26 μA , and the energetic materials were isolated from all peripheral electrical system effects completely.

Author Contributions: In this paper, H.F. collected information on self-destruction system designs and the process of developing an insurance actuator and cooper azide. W.L. carried out research on the insurance improvement mechanism of energetic materials. B.H. carried out the insurance actuator mechanical response model calculation and numerical analysis. S.L. and W.S. finished the match test on the insurance actuator & cooper azide. All authors have read and agreed to the published version of the manuscript.

Funding: This work was supported by the China Postdoctoral Science Foundation (70th) [grant numbers: 2021M700419].

Data Availability Statement: All other data are available from the corresponding authors upon reasonable request.

Conflicts of Interest: The authors declare that there are no conflict of interest regarding the publication of this paper.

References

1. Han, J.-W.; Seol, M.-L.; Choi, Y.-K.; Meyyappan, M. Self-destructible fin flip-flop actuated channel transistor. *IEEE Electron Device Lett.* **2016**, *37*, 130–133. [[CrossRef](#)]
2. Tada, S.; Yamashita, Y.; Matsuda, K.; Nagata, M.; Sakiyama, K.; Miura, N. Design and concept proof of an inductive impulse self-destructor in sense-and-react countermeasure against physical attacks. *Jpn. J. Appl. Phys.* **2021**, *60*, SBBL01. [[CrossRef](#)]

3. Federal Ministry of Education and Research. The German Federal Government's Framework Programme for Research and Innovation 2021–2024. Available online: https://www.bundesbericht-forschung-innovation.de/files/BMBF_BuFI-2020_Short-version.pdf (accessed on 10 April 2022).
4. Szondy, D. DARPA Investigating Self-destructing Electronics. Available online: <https://newatlas.com/vapr-transient-electronics/26004/> (accessed on 11 April 2022).
5. Alsobrooks, M.E. Vanishing Programmable Resource: Design, Materials and Characterization. Available online: https://www.nnin.org/sites/default/files/2015_REU/2015NNINreuRA_PDFs/2015NNINreuRA_Alsobrooks.pdf (accessed on 9 April 2022).
6. Hwang, S.W.; Rogers, J.A. A physically transient form of silicon electronics. *Science* **2012**, *337*, 1640–1644. [[CrossRef](#)] [[PubMed](#)]
7. Fleck, T.J.; Ramachandran, R.; Murray, A.K.; Novotny, W.A.; Chiu, G.T.C.; Gunduz, I.E.; Son, S.F.; Rhoads, J.F. Controlled Substrate Destruction Using Nanothermite. *Propellants Explos. Pyrotech.* **2017**, *42*, 579–584. [[CrossRef](#)]
8. Nicollet, A.; Salvagnac, L.; Baijot, V.; Estève, A.; Rossi, C. Fast circuit breaker based on integration of Al/CuO nanothermites. *Sens. Actuators A Phys.* **2018**, *273*, 249–255. [[CrossRef](#)]
9. Bouangeune, D.; Lee, Y.J. Transient voltage suppressor diode designed for the protection of high-brightness GaN-based LEDs from various electrostatic discharge shocks. *J. Korean Phys. Soc.* **2014**, *65*, 1106–1112. [[CrossRef](#)]
10. Mardiguian, M. *Electrostatic Discharge: Understand, Simulate and Fix ESD Problems*, 3rd ed.; Wiley: Hoboken, NJ, USA, 2009; p. 30.
11. Liu, F.; Gao, S.; Han, H.; Tian, Z.; Liu, P. Interference reduction of high energy noise for modal parameter identification of offshore wind turbines based on iterative signal extraction. *Ocean. Eng.* **2019**, *183*, 372–383. [[CrossRef](#)]
12. Li, Z.; Goebel, K.; Wu, D. Degradation modeling and remaining useful life prediction of aircraft engines using ensemble learning. *ASME Trans. J. Eng. Gas Turbines Power* **2018**, *141*, 041008. [[CrossRef](#)]
13. Bouangeune, D.; Vilathong, S.; Cho, D.-H.; Shim, K.-H.; Leem, S.-J.; Choi, C.-J. Novel punch-through diode triggered SCR for low voltage ESD protection applications. *J. Semicond. Technol.* **2014**, *14*, 797–801. [[CrossRef](#)]
14. Bouangeune, D.; Choi, S.-S.; Choi, C.-J.; Cho, D.-H.; Shim, K.-H. Bidirectional transient voltage suppression diodes for the protection of high speed data line from electrostatic discharge shocks. *J. Semicond. Technol.* **2014**, *14*, 1–7. [[CrossRef](#)]
15. Salcedo, J.A.; Hajjar, J.-J.; Malobabic, S.; Liou, J.J. Bidirectional devices for automotive-grade electrostatic discharge applications. *IEEE Electron. Device Lett.* **2012**, *33*, 860–862. [[CrossRef](#)]
16. Liu, Z.; Vinson, J.; Lou, L.; Liou, J.J. An improved bidirectional SCR structure for low-triggering ESD protection applications. *IEEE Electron. Device Lett.* **2008**, *29*, 360–362.
17. Bouangeune, D.; Cho, D.-H.; Yun, H.-J.; Shim, K.-H.; Choi, C.-J. Transmission line pulse properties for a bidirectional transient voltage suppression diode fabricated using low-temperature epitaxy. *Electron. Mater. Lett.* **2015**, *11*, 88–92. [[CrossRef](#)]
18. Chundru, R.; Li, Z.; Pommerenke, D.; Kam, K.; Lam, C.-W.; Centola, F.; Steinfeld, R. An evaluation of TVS devices for ESD protection. In Proceedings of the IEEE International Symposium on Electromagnetic Compatibility, Long Beach, CA, USA, 14–19 August 2011; p. 62.
19. Feng, H.; Lou, W. Design, Processing and Testing of a MEMS Energy Grooming Structure for Initiator Materials. *IEEE Access* **2019**, *7*, 93150–93610. [[CrossRef](#)]
20. Chua, B.; Wexler, A.; Tien, N.; Niemeier, D.; Holmen, B. Design, fabrication and testing of a microfabricated corona ionizer. *J. Microelectromech. Syst.* **2008**, *17*, 115–138. [[CrossRef](#)]
21. Marciulionis, P. Analysis of space charge distribution in dc corona discharge field computed with finite element method. *IEEE Trans. Plasma Sci.* **2017**, *45*, 1698–1703. [[CrossRef](#)]
22. Lou, W.; Feng, H. Research on fuze microswitch based on corona discharge effect. *Def. Technol.* **2020**, *17*, 1453–1460. [[CrossRef](#)]
23. Singh, K. Substrate material considerations in MEMS processes for RF applications. *NANO Microsyst. Technol.* **2017**, *19*, 422–431. [[CrossRef](#)]
24. Tirumala, R.; Li, Y. Corona discharges in sub-millimeter electrodes gaps. *J. Electros.* **2011**, *69*, 36–42. [[CrossRef](#)]
25. Bachtold, A.; Hadley, P.; Nakanishi, T.; Dekker, C. Logic circuits with carbon nanotube transistors. *Science* **2001**, *294*, 1317–1320. [[CrossRef](#)]
26. Brice, C.W.; Dougal, R.A.; Hudgins, J.L. Review of technologies for current-limiting low-voltage circuit breakers. *IEEE Trans. Ind. Appl.* **1996**, *32*, 1005–1010. [[CrossRef](#)]
27. Konofaos, N.; Voilas, T.K.; Alexiou, G.P. Defect related effects on the reliability and performance of an embedded DRAM cell designed with MOSFETs with alternative gate dielectrics. *J. Phys. Conf. Ser.* **2005**, *10*, 365. [[CrossRef](#)]
28. Liu, H.; Koh, K.H.; Lee, C. Ultra-wide frequency broadening mechanism for micro-scale electromagnetic energy harvester. *Appl. Phys. Lett.* **2014**, *104*, 053901. [[CrossRef](#)]
29. Liu, H.; Tay, C.J.; Quan, C.; Kobayashi, T.; Lee, C. A scrape-through piezoelectric MEMS energy harvester with frequency broadband and up-conversion behaviors. *Microsyst. Technol.* **2011**, *17*, 1747–1754. [[CrossRef](#)]
30. Sevely, F.; Charlot, S.; Séguier, L.; Mesnilgrete, F.; Rossi, C. Design, Fabrication and Testing of a Miniaturized end-of-life Ultimate Security Device Using Reactive Composites. In Proceedings of the 45th International Pyrotechnics Society Seminar, Colorado Springs, CO, USA, 10–15 July 2022.